Adsorption Equilibrium of Binary Mixtures of Carbon Dioxide and Water Vapor on Zeolites 5A and 13X

Yu Wang and M. Douglas LeVan*

Department of Chemical and Biomolecular Engineering, Vanderbilt University, Nashville, Tennessee 37235

Adsorption equilibria were measured for binary mixtures of carbon dioxide and water vapor on zeolites 5A and 13X using a volumetric apparatus. The experiments were conducted at (0, 25, and 50) °C with water loadings of (1.0, 3.4, and 9.4) mol·kg^{-1}. With an increase in adsorbed water loadings, the loadings of weakly adsorbed CO_2 decrease appreciably. Pure component data are described well by a multitemperature Toth isotherm. Binary data show a discrepancy with predictions of the ideal adsorbed solution theory (IAST) but are described well by a virial excess mixing coefficient (VEMC) model, which adds corrective terms to the IAST to account for nonidealities. Data measured at lower CO_2 partial pressures and higher water loadings show indications of chemisorption and carbonate formation.

Introduction

The emission of CO_2 from the combustion of fossil fuels is the major reason for the accumulation of CO_2 in the atmosphere and is contributing significantly to global warming.[1] Also, the need to remove water vapor and carbon dioxide from air is encountered in many applications such as air separation, purification, environmental protection, and spacecraft atmosphere revitalization.[2] Adsorption is one of the technologies used to address these issues and is targeted for expanded applications. Impurities like water vapor and carbon dioxide will detrimentally affect the capacity of adsorbents used for separation or purification.[3] Therefore, equilibrium information for water vapor and carbon dioxide is needed for process designs. However, experimental equilibrium data over a broad range of temperatures and concentrations, especially mixture equilibrium data, are extremely scarce.

Zeolites are selective adsorbents for the removal of carbon dioxide, water vapor, and other impurities from mixtures. Water is a strongly adsorbed component on zeolite. Thus, a trace amount of water vapor will dramatically affect the adsorption of CO_2 by the zeolite. Because of insufficient data for these systems, an understanding of the effect of water on the coadsorption of carbon dioxide is largely lacking.[4,5]

The mechanism of CO_2 adsorption on zeolites has been studied and is reported to involve both physical adsorption and chemisorption.[6−8] Bertsch and Habgood[6] measured infrared spectra of small amounts of water and CO_2 up to one molecule per cavity adsorbed on LiX, NaX, and KX zeolites. The adsorption of CO_2 appears to involve both physical adsorption in a linear configuration at a cation, which is the major part of the adsorption occurring at higher pressures, and chemisorption in one or more bent configurations, which is thought to involve the formation of carbonate ions by interaction with surface oxide groups. The authors suggested that there is little chemisorption beyond approximately 0.5 to 1 molecule per cavity, and consequently chemisorption would not be readily detectable from normal isotherm measurements. Also, they studied the interaction of water and carbon dioxide on the zeolite surface and showed that the presence of roughly equivalent amounts of water and carbon dioxide greatly increases the rate of carbon dioxide chemisorption in the low concentration range. Montanari and Busca[7] used IR spectroscopy to investigate the mechanism of adsorption and separation of CO_2 on zeolites 3A, 4A, and 5A and found that CO_2 adsorption in the form of both linear molecular species and carbonate species occurs mostly at the external surface of 3A zeolite and in the cavities of 4A and 5A zeolites.

Baltrusaitis et al.[9,10] investigated CO_2 adsorption at the adsorbed water/iron oxide interface under ambient conditions. They reported Fourier transform infrared (FTIR) spectra for CO_2 adsorption in the presence and absence of coadsorbed water on hydroxylated nanoparticulate Fe_2O_3 and γ-Al_2O_3 at 296 K. They concluded that CO_2 can react with surface OH groups to form adsorbed bicarbonate on the surface in the absence of coadsorbed water, and CO_2 reacts with adsorbed water to yield adsorbed carbonate and protonated surface hydroxyl groups with coadsorbed water instead. They proposed a mechanism for surface reactions of CO_2 at the adsorbed water−oxide interface.

Li et al.[11] studied adsorption equilibria for a binary mixture of CO_2 and H_2O on activated alumina at several temperatures and over a wide range of concentrations (4 % to 90 % of the saturated water vapor pressure). They found that the adsorption of H_2O was mildly depressed by competition from CO_2 at lower relative humidity and that the loading of CO_2 is almost unchanged with only a slight decrease at higher water humidity.

Rege and Yang[4] developed a FTIR method to study the binary adsorption of CO_2 and H_2O at low concentrations on two adsorbents, 13X zeolite and γ-Al_2O_3. Their results show a distinct enhancement in the amount of CO_2 adsorbed at low concentrations with H_2O present in trace amounts. The enhancement gradually decreased and finally disappeared as the CO_2 partial pressure increased. The reason for the enhancement in CO_2 adsorption was unknown and was explained by two possibilities: catalysis of the formation of bicarbonate species on the sorbent surface by adjacent H_2O molecules or enhancement in adsorbate diffusion due to the occupation of high energy sites by water molecules.[4] The experimental mixture data were fit to the Doong−Yang model and also as an ideal adsorbed solution to the Dubinin−Astakhov equation. The Doong−Yang model gave a marginally better description. Both models underpredicted CO_2 adsorption at very low partial pressures in

* To whom correspondence should be addressed. Mailing address: Vanderbilt University, VU Station B 351604, 2301 Vanderbilt Place, Nashville, TN 37235-1604 USA. Tel.: (615) 343-1672. Fax: (615) 343-7951. E-mail: m.douglas.levan@vanderbilt.edu.

10.1021/je100053g
Published on Web 06/04/2010

the presence of trace amounts of moisture. As an alternative finding, Brandani and Ruthven[5] showed that small amounts of water inhibit the adsorption of CO_2 on several different cationic forms of zeolite X (NaLSX, LiLSX, and CaX) using the zero length column technique.

In our previous paper,[12] we reported pure component isotherms for water vapor and carbon dioxide on zeolites 13X and 5A over the temperature ranges of (−45 to 175) °C. The measurement was accomplished by using a volumetric adsorption apparatus with a circulation pump in a closed loop design to accelerate the attainment of equilibrium. The isotherms are described well by a Toth model with parameters having temperature dependence.

Binary isotherms of water vapor and carbon dioxide are reported in this paper. The binary adsorption data were measured on zeolites 13X and 5A using our volumetric adsorption apparatus at the three water loadings of (1.0, 3.4, and 9.4) $mol \cdot kg^{-1}$ and temperatures of (0, 25, and 50) °C. The ideal adsorbed solution theory (IAST) and viral excess mixture coefficient (VEMC) model in conjunction with the Toth isotherm model are applied and compared to describe the mixture equilibria.

Isotherm Models. The adsorption of water vapor and carbon dioxide as pure components on zeolites 13X and 5A is described well by a Toth model with temperature-dependent parameters[12]

$$\theta = \frac{n}{n_s} = \frac{bP}{[1 + (bP)^t]^{1/t}} \tag{1}$$

where n_s is the saturation capacity, b is an equilibrium constant, and t characterizes heterogeneity of the adsorbent. For the temperature dependence, b takes a general form of the adsorption affinity

$$b = b_0 \exp(E/T) \tag{2}$$

and t has the empirical functional form[13]

$$t = t_0 + a/T \tag{3}$$

The IAST has been reviewed extensively in the literature[14−16] and has been successfully applied to ideal mixtures. The fundamental requirement for adsorption is the mixing of components at a common spreading pressure π. For a pure component, spreading pressure is calculated using

$$\frac{\pi A}{RT} = \int_0^{P_i^0} \frac{n_i}{P_i} \, dP_i \tag{4}$$

For the ideal adsorbed solution, the relationship between the adsorbed and the bulk phase is described by the analogous Raoult's law relationship

$$P_i = y_i P = x_i P_i^0(\pi) \tag{5}$$

where $P_i^0(\pi)$ is the partial pressure of pure component i, calculated using eq 4, at the spreading pressure and temperature of the mixture.

The total adsorbed-phase loading n_T is calculated from

$$\frac{1}{n_T} = \sum_{i=1}^{N} \frac{x_i}{n_i^0} \tag{6}$$

where $n_i^0(P_i^0)$ is the amount adsorbed in the standard state calculated from the pure component isotherm. Quantities of individual components adsorbed are given by

$$n_i = x_i n_T \tag{7}$$

In the IAST model, pure component isotherms can be of any physically meaningful form. Here, the Toth model with the temperature-dependent parameters[12] is used.

The IAST assumes that the adsorbed phase forms an ideal solution, and therefore it will provide a better description for ideal or nearly ideal systems than for nonideal systems. Various approaches have been developed to correct for the deviation of a real adsorbed solution from an ideal adsorbed solution. Among them, the VEMC model is promising as a general approach to describe multicomponent adsorption equilibria for both nonideal and ideal systems.[17,18] The model attributes the mixture adsorption equilibrium to contributions from an ideal adsorbed solution and corrections for nonideality based on excess mixture coefficients developed through the two-dimensional virial equation of state (EOS) approach. Multicomponent adsorption equilibria can be described by the two-dimensional virial equation

$$\frac{\pi A}{RT} = n + \frac{1}{A}\sum_i \sum_j n_i n_j B_{ij} + \frac{1}{A^2}\sum_i \sum_j \sum_k n_i n_j n_k C_{ijk} + \ldots \tag{8}$$

where A is the specific surface area of the adsorbent and B_{ij}, C_{ijk}, and so forth are the virial coefficients.

Rearranging eq 8 for a binary system to group terms for pure components and the mixture gives

$$\begin{aligned}\frac{\pi A}{RT} = {} & n_1 + \frac{1}{A}B_{11}n_1^2 + \frac{1}{A^2}C_{111}n_1^3 + \ldots \\ & + n_2 + \frac{1}{A}B_{22}n_2^2 + \frac{1}{A^2}C_{222}n_2^3 + \ldots \\ & + \frac{2}{A}B_{12}n_1n_2 + \frac{3}{A^2}C_{112}n_1^2n_2 + \frac{3}{A^2}C_{122}n_2^2n_1 + \ldots\end{aligned} \tag{9}$$

With surface mixing considered to arise from an ideal surface mixing contribution and an excess surface mixing contribution, the virial coefficients can be written

$$B_{ij} = B_{ij}^{id} + B_{ij}^{E} \qquad (i \neq j) \tag{10}$$

$$C_{ijk} = C_{ijk}^{id} + C_{ijk}^{E} \qquad (i = j \neq k;\ i \neq j = k) \tag{11}$$

where B_{ij}^{id} and C_{ijk}^{id} are the virial ideal mixing coefficients, which represent the contributions from the ideal adsorbed solution, and B_{ij}^{E} and C_{ijk}^{E} are the virial excess mixing coefficients, which represent the contributions that describe the deviation of a real adsorbed solution from the ideal adsorbed solution. Collecting terms and rewriting eq 9 gives

$$\begin{aligned}\frac{\pi A}{RT} &= \left.\frac{\pi A}{RT}\right|_{pure1} + \left.\frac{\pi A}{RT}\right|_{pure2} + \left.\frac{\pi A}{RT}\right|^{id}_{mixing} + \left.\frac{\pi A}{RT}\right|^{E}_{mixing} \\ &= \left.\frac{\pi A}{RT}\right|_{IAS} + \left.\frac{\pi A}{RT}\right|^{E}_{mixing} \\ &= \left.\frac{\pi A}{RT}\right|_{IAS} + \frac{2}{A}B_{12}^{E}n_1n_2 + \frac{3}{A^2}C_{112}^{E}n_1^2n_2 + \\ &\qquad \frac{3}{A^2}C_{122}^{E}n_2^2n_1 + \ldots\end{aligned} \tag{12}$$

where the terms on the right side are contributions to the spreading pressure of the mixture.

The VEMC model describes the nonideal multicomponent adsorption equilibrium through the IAST with a correction using VEMCs. The equations for a binary mixture are[18]

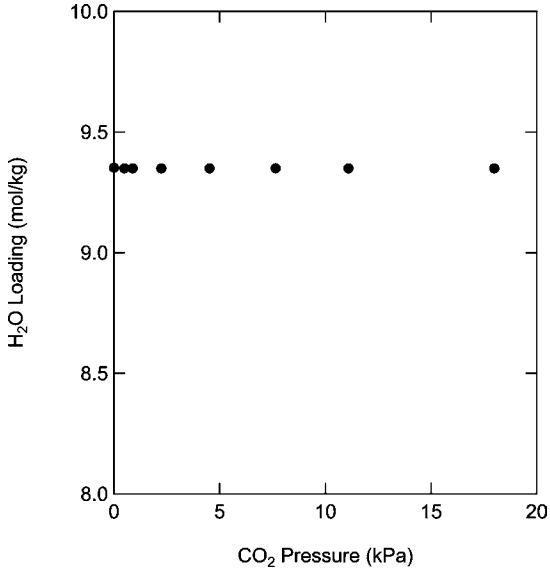

Figure 1. Impact of CO_2 on H_2O coadsorption.

$$\ln P_1 = \ln P_{IAS1} + \frac{2}{A}B_{12}^{E}n_2 + \frac{3}{A^2}C_{112}^{E}n_1n_2 + \frac{3}{2A^2}C_{122}^{E}n_2^{\,2} + \ldots \quad (13)$$

$$\ln P_2 = \ln P_{IAS2} + \frac{2}{A}B_{12}^{E}n_1 + \frac{3}{A^2}C_{122}^{E}n_1n_2 + \frac{3}{2A^2}C_{112}^{E}n_1^{\,2} + \ldots \quad (14)$$

The leading term on the right-hand side is the contribution from the IAST model, and the latter terms involving the corrective terms *B* and *C* give the contribution from nonideal mixing. For an ideally mixed system, these corrective terms will be zero. Thus, the VEMC model will reduce to IAST for this limiting case.

Experimental Section

Materials. The adsorbents used in this study, manufactured by the Davison Chemical Division of W. R. Grace, are zeolite 5A (MS 522) and zeolite 13X (MS 544HP). Both were in the form of 8 × 12 mesh spherical beads. CO_2 (99.6 %) was obtained from J&M Cylinder Gases. Helium (99.995 %) was supplied by Air Liquide.

Apparatus and Operating Procedures. We constructed a volumetric apparatus to measure adsorption isotherms for pure carbon dioxide, water vapor, and their binary mixtures. A schematic of the apparatus and complete operating information can be found in the previous paper.[12]

For binary isotherm measurements of carbon dioxide and water vapor, the loading of water was held essentially constant while increasing the loadings of the CO_2 to obtain isotherms. This was possible because water vapor is much more strongly adsorbed, and the amount of water vapor in the loop remains constant. Water vapor pressures could not be measured in some of our experiments because the partial pressure for water vapor was too low.

The zeolite samples were in spherical bead form and contained a clay binder. We report adsorption capacities based on the total weight of the zeolite samples with the binder. On the basis of data available in the trade literature from W. R. Grace, the samples contain about 20 % binder by weight. The specific surface area of the binder is low compared to those of the zeolites, and thus adsorption of carbon dioxide and water in the binder can be assumed to be very small compared to that in the zeolites.

The quantity of water needed to obtain a desired loading for a given sample weight was injected and equilibrated in the adsorption bed first; then a series of CO_2 injections were made, and gas-phase concentrations were analyzed using a gas chromatograph (HP 6890). On the basis of the standard operating principles of a volumetric system, the quantities of adsorbed CO_2 were obtained by subtracting the amount remaining in the vapor phase from the amount injected.

Results and Discussion

The binary adsorption of water vapor and carbon dioxide was measured on zeolite 13X and 5A at (0, 25, and 50) °C. The mixture measurements were conducted with water loadings held constant at (1.0, 3.4, and 9.4) mol·kg^{-1}. To verify this assumption of constant water loading, we measured water partial pressures as we repeatedly injected more CO_2 into the system with an initial water loading of 9.4 mol·kg^{-1} and temperature of 50 °C. The results, shown in Figure 1, clearly demonstrate that the adsorbed-phase concentration is essentially constant, varying only 0.03 % from the initial pure water loading when the CO_2 pressures increased in the system. This indicates that the water loadings were not affected by the coadsorption of CO_2 and can be assumed constant for the study.

All experimental measurements were repeated to verify the precision of the data. From different sets of data, the relative errors in CO_2 loadings were determined based on standard deviations. The maximum relative error for the water loading of 1 mol·kg^{-1} was less than 3 % for both zeolites. For the water loading of 3.4 mol·kg^{-1}, the maximum relative errors for all temperatures and both zeolites averaged 8 %. For the water loading of 9.4 mol·kg^{-1} on 13X zeolite, the maximum relative error was 5 %.

The experimental equilibrium data for zeolite 13X are listed in Table 1. Figures 2 to 4 show pure and binary CO_2 isotherms

Table 1. Adsorption Equilibria of Binary CO_2 and H_2O on Zeolite 13X[a]

n_{water} = 1.0 mol·kg^{-1}						n_{water} = 3.4 mol·kg^{-1}						n_{water} = 9.4 mol·kg^{-1}					
0 °C		25 °C		50 °C		0 °C		25 °C		50 °C		0 °C		25 °C		50 °C	
p	*n*	*p*	*n*	*p*	*n*	*p*	*n*	*p*	*n*	*p*	*n*	*p*	*n*	*p*	*n*	*p*	*n*
0.335	0.941	0.368	0.533	0.651	0.346	0.554	0.430	1.788	0.358	0.914	0.1085	1.110	0.1605	2.844	0.1245	2.239	0.0603
1.23	1.57	1.46	0.885	1.64	0.508	1.29	0.659	3.549	0.527	1.928	0.156	2.101	0.2362	4.962	0.1769	4.522	0.0905
2.98	2.15	4.32	1.41	3.11	0.697	3.33	1.08	8.09	0.804	3.42	0.202	3.519	0.3027	7.57	0.2193	7.65	0.1227
6.84	2.74	9.99	1.90	6.00	0.94	14.4	1.78	23.63	1.249	6.67	0.278	6.65	0.430	13.08	0.298	11.09	0.1485
19.5	3.34	25.5	2.37	10.8	1.22					11.92	0.368					17.99	0.1999
				17.9	1.50												
				27.1	1.80												

[a] Unit: *p* (kPa) and *n* (mol·kg^{-1}).

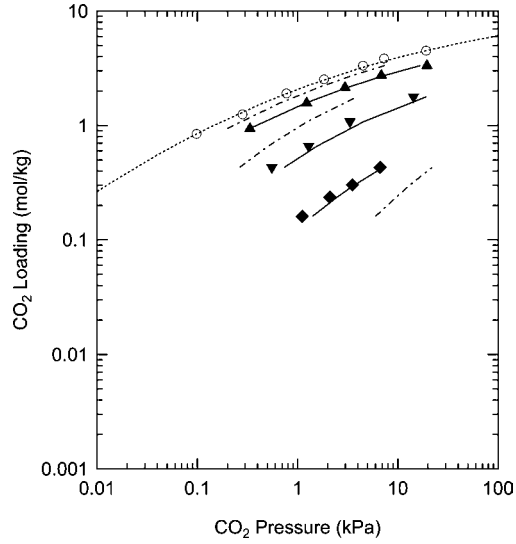

Figure 2. CO_2 adsorption isotherms on zeolite 13X at 0 °C: ○, pure CO_2; ▲, binary CO_2 with 1 mol·kg^{-1} H_2O; ▼, binary CO_2 with 3.4 mol·kg^{-1} H_2O; ◆, binary CO_2 with 9.4 mol·kg^{-1} H_2O; dotted curve is the Toth isotherm for pure CO_2; dashed curves are the IAST model; and solid curves are the VEMC model for mixtures.

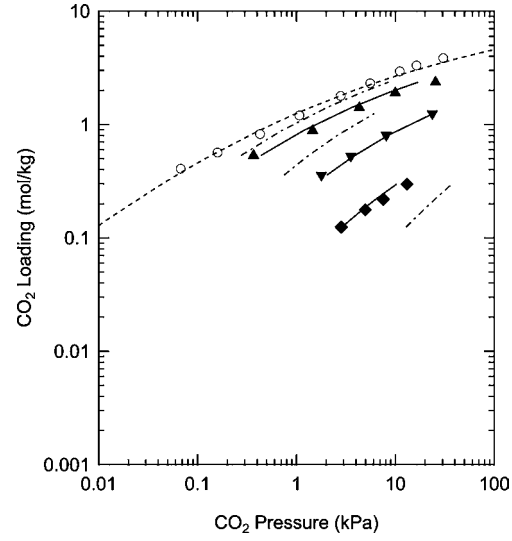

Figure 3. CO_2 adsorption isotherms on zeolite 13X at 25 °C: ○, pure CO_2; ▲, binary CO_2 with 1 mol·kg^{-1} H_2O; ▼, binary CO_2 with 3.4 mol·kg^{-1} H_2O; ◆, binary CO_2 with 9.4 mol·kg^{-1} H_2O; dotted curve is the Toth isotherm for pure CO_2; dashed curves are the IAST model; and solid curves are the VEMC model for mixtures.

on zeolite 13X at (0, 25, and 50) °C. The circle symbols at the top of the figures represent pure CO_2 isotherm data from our previous paper,[12] and other filled symbols represent binary CO_2 isotherm data. The capacities for binary CO_2 adsorption are lower than for pure CO_2. Thus, it is clear that CO_2 and H_2O adsorb competitively for the concentration range investigated. This agrees with the finding of Brandani and Ruthven that small amounts of water inhibit the adsorption of CO_2.[5] Furthermore, CO_2 loadings decrease with increasing water loadings. When water is preloaded at 1.0 mol·kg^{-1}, the CO_2 capacities drop more than 30 % compared to pure component CO_2 adsorption. With preloaded water loadings increasing to (3.4 and 9.4) mol·kg^{-1}, the CO_2 capacities continue to drop more than 50 % and 80 %, respectively.

To estimate how the humidity of air interferes with CO_2 adsorption, we can convert the water loading to its equilibrated pressure using the pure water vapor isotherm. For water loadings

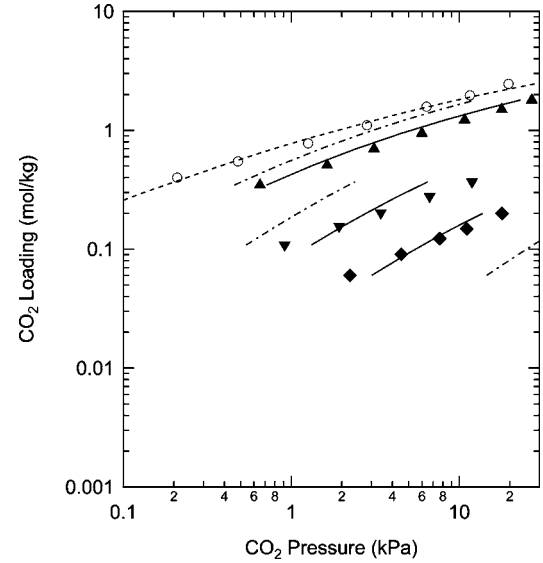

Figure 4. CO_2 adsorption isotherms on zeolite 13X at 50 °C: ○, pure CO_2; ▲, binary CO_2 with 1 mol·kg^{-1} H_2O; ▼, binary CO_2 with 3.4 mol·kg^{-1} H_2O; ◆, binary CO_2 with 9.4 mol·kg^{-1} H_2O; dotted curve is the Toth isotherm for pure CO_2; dashed curves are the IAST model; and solid curves are the VEMC model for mixtures.

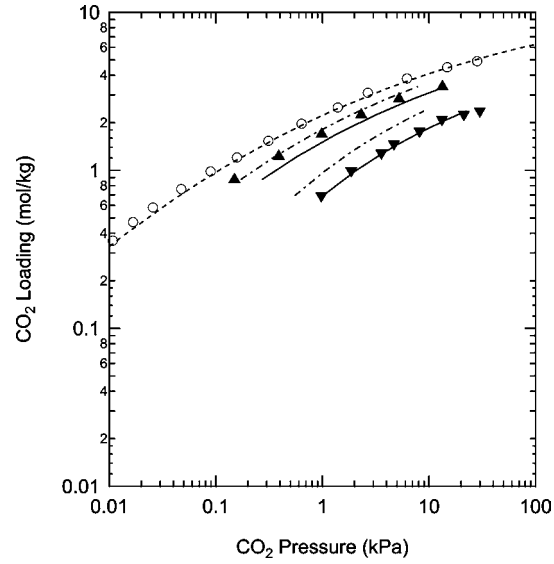

Figure 5. CO_2 adsorption isotherms on zeolite 5A at 0 °C: ○, pure CO_2; ▲, binary CO_2 with 1 mol·kg^{-1} H_2O; ▼, binary CO_2 with 3.4 mol·kg^{-1} H_2O; dotted curve is the Toth isotherm for pure CO_2; dashed curves are the IAST model; and solid curves are the VEMC model for mixtures.

at (1.0, 3.4, and 9.4) mol·kg^{-1} at 25 °C on 13X, the corresponding equilibrium water vapor pressures are ($9.1 \cdot 10^{-5}$, $8.5 \cdot 10^{-4}$, and $4.3 \cdot 10^{-2}$) kPa, respectively.[12] Considering that the saturated water vapor pressure is 3.169 kPa at 25 °C,[19] the relative humidity is below 1.4 %, even for the water loading of 9.4 mol·kg^{-1}. It is clear that the CO_2 removal capability can be dramatically affected even by a small amount of water vapor in air.

Pure and binary CO_2 isotherms on zeolite 5A at different temperatures have a similar trend as shown in Figures 5 to 7, with the data tabulated in Table 2. The figures show that CO_2 adsorption capacities decrease dramatically when the water loadings increase. Even for 0.02 % relative humidity at room temperature, corresponding to 3.4 mol·kg^{-1} of H_2O, the CO_2 adsorption can drop more than 50 % compared to dry conditions.

It is of interest to understand the performance of predictive models for mixture adsorption because of the limited availability

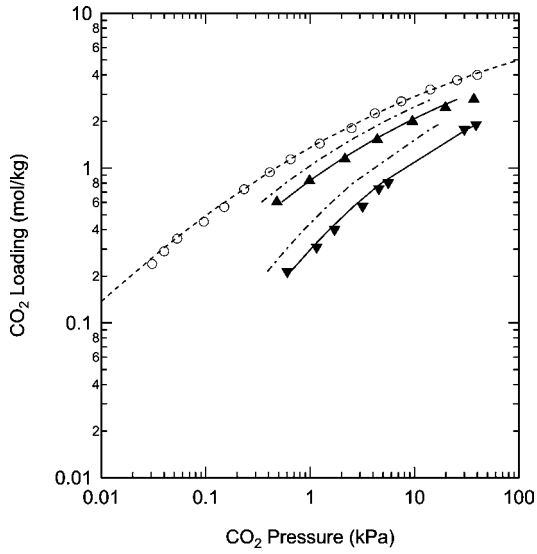

Figure 6. CO_2 adsorption isotherms on zeolite 5A at 25 °C: ○, pure CO_2; ▲, binary CO_2 with 1 mol·kg^{-1} H_2O; ▼, binary CO_2 with 3.4 mol·kg^{-1} H_2O; dotted curve is the Toth isotherm for pure CO_2; dashed curves are the IAST model; and solid curves are the VEMC model for mixtures.

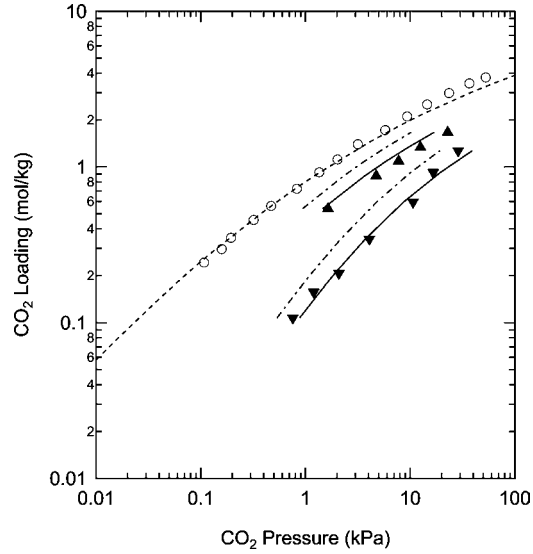

Figure 7. CO_2 adsorption isotherms on zeolite 5A at 50 °C: ○, pure CO_2; ▲, binary CO_2 with 1 mol·kg^{-1} H_2O; ▼, binary CO_2 with 3.4 mol·kg^{-1} H_2O; dotted curve is the Toth isotherm for pure CO_2; dashed curves are the IAST model; and solid curves are the VEMC model for mixtures.

of mixture equilibrium data. Here, we compare our experimental data with the IAST with pure components described by the Toth isotherm model. The parameters of the pure component Toth model are given in Table 3. The IAST predictions are shown by the long and short dashed lines in Figures 2 to 7. At the low water loading of 1.0 mol·kg^{-1}, the prediction from IAST is close but above the data. With increasing water loadings, however, the discrepancy between the prediction and the data increases. This implies that the binary system behaves significantly nonideally, which cannot be described well with the IAST model. Thus, a model considering nonideal behavior needs to be applied.

Table 3. Parameters for the Single-Component Toth Isotherm[12]

	a_0	b_0	E		c
system	mol·kg^{-1}·kPa^{-1}	kPa^{-1}	K	t_0	K
CO_2/13X	$6.509\cdot10^{-3}$	$4.884\cdot10^{-4}$	$2.991\cdot10^{3}$	$7.487\cdot10^{-2}$	$3.805\cdot10^{1}$
H_2O/13X	$3.634\cdot10^{-6}$	$2.408\cdot10^{-7}$	$6.852\cdot10^{3}$	$3.974\cdot10^{-1}$	-4.199
CO_2/5A	$9.875\cdot10^{-7}$	$6.761\cdot10^{-8}$	$5.625\cdot10^{3}$	$2.700\cdot10^{-1}$	$-2.002\cdot10^{1}$
H_2O/5A	$1.106\cdot10^{-8}$	$4.714\cdot10^{-10}$	$9.955\cdot10^{3}$	$3.548\cdot10^{-1}$	$-5.114\cdot10^{1}$

Table 4. VEMC Parameters and Normalized Error for IAST and VEMC Models for Binary Mixtures of CO_2 with H_2O

parameter	13X system	5A system
B^E_{12}/A (kg·mol^{-1})	0.23	0.26
C^E_{112}/A^2 (kg·mol^{-1})^2	$4.10\cdot10^{-2}$	$1.84\cdot10^{-2}$
C^E_{122}/A^2 (kg·mol^{-1})^2	$-4.18\cdot10^{-2}$	$-7.60\cdot10^{-2}$
ε_{IAST}	16.6	10.1
ε_{VEMC}	3.4	3.3

We use the VEMC model to take account of nonideality and describe the binary isotherms at different temperatures and water loadings simultaneously. The VEMC parameters (B^E_{12}, C^E_{112}, and C^E_{122}) were determined by minimizing the objective function[17]

$$e = \sum_m (\ln p^{cal}_{m,CO_2} - \ln p^{exp}_{m,CO_2})^2 \qquad (15)$$

where p^{exp}_{m,CO_2} is the measured partial pressure of CO_2 with data index m and p^{cal}_{m,CO_2} is the CO_2 pressure calculated using eq 13. The normalized error ε was defined to evaluate model accuracy[17]

$$\varepsilon = \frac{100}{M}\sqrt{e} \qquad (16)$$

where M is the total number of mixture data at different temperatures and water loadings.

The fitted VEMC parameters for both systems are listed in Table 4. The CO_2 isotherms with preloaded water were calculated with these VEMC parameters and are plotted as the solid curves shown in Figures 2 to 7. It is clear that the VEMC model can describe the binary CO_2 data well for different temperatures and water loadings with only three additional parameters for each adsorbent. Comparisons of the experimentally measured partial pressures and calculated partial pressures for CO_2 using the VEMC and IAST models are shown in Figures 8 and 9 for the 13X and 5A systems, respectively. The

Table 2. Adsorption Equilibria of Binary CO_2 and H_2O on Zeolite 5A[a]

n_{water} = 1.0 mol·kg^{-1}						n_{water} = 3.4 mol·kg^{-1}					
0 °C		25 °C		50 °C		0 °C		25 °C		50 °C	
p	n	p	n	p	n	p	n	p	n	p	n
0.149	0.874	0.480	0.604	1.644	0.539	0.976	0.691	0.6048	0.2145	0.758	0.1075
0.389	1.23	0.986	0.829	4.74	0.875	1.863	0.994	1.155	0.308	1.200	0.158
0.984	1.70	2.16	1.14	7.76	1.090	3.574	1.288	1.714	0.401	2.09	0.207
2.31	2.25	4.40	1.53	12.55	1.34	4.69	1.472	3.18	0.567	4.08	0.343
5.23	2.84	9.54	2.00	22.9	1.67	8.16	1.77	4.56	0.738	10.66	0.594
13.4	3.39	19.8	2.46			13.21	2.10	5.59	0.805	16.6	0.920
		37.1	2.78			21.22	2.26	30.07	1.783	28.8	1.270
						29.9	2.38	38.85	1.908		

[a] Unit: P (kPa) and n (mol·kg^{-1}).

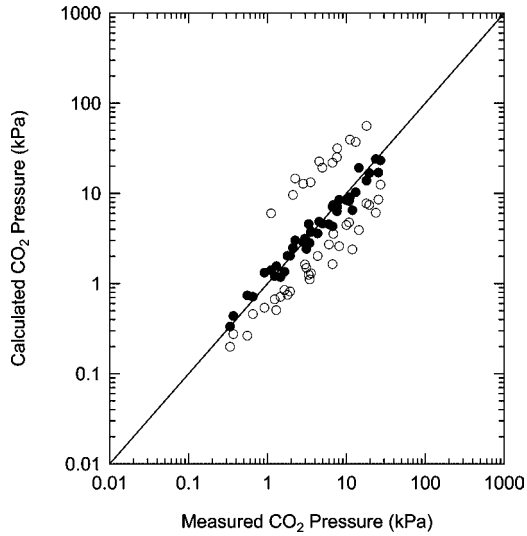

Figure 8. Binary adsorption equilibria of CO_2 and H_2O on zeolite 13X at (0, 25, and 50) °C using the IAST and VEMC models: ○, IAST; ●, VEMC.

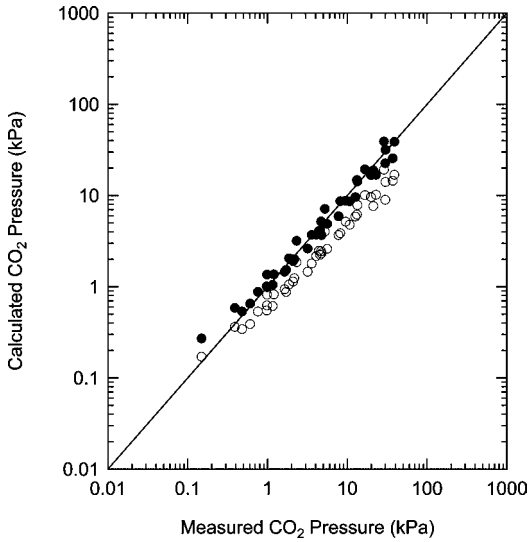

Figure 9. Binary adsorption equilibria of CO_2 and H_2O on zeolite 5A at (0, 25, and 50) °C using the IAST and VEMC models: ○, IAST; ●, VEMC.

normalized errors ε, calculated with the IAST and VEMC models, are given in the Table 4. The lower the value of ε is, the more accurate is the model description. For both systems, the VEMC model shows a strong improvement over the IAST model.

We did not include experimental data in our tables and figures for low CO_2 partial pressures for both zeolites and for a water loading of 9.4 mol·kg^{-1} on zeolite 5A. These data show much flatter slopes than theoretical Henry's law slopes in the low CO_2 partial pressure region and, based on the material balance for the volumetric system, appear to have much higher loadings compared to model predictions. This trend became more obvious with increasing water loadings and temperatures. We believe that it is caused by preadsorbed water vapor helping to catalyze CO_2 chemisorption and leading to the formation of carbonates under these conditions.

Similar observations have been given by previous researchers as discussed in the introduction.[1,6−9,20] In particular, prior evidence exists for a loading dependence for chemisorption and carbonate formation. Bertsch and Habgood[6] used IR spectra to study the interaction of water and carbon dioxide (up to one molecule per cavity) on the Linde zeolite NaX surface and reported that the presence of roughly equivalent amounts of water greatly increases the rate of CO_2 chemisorption for low CO_2 concentrations. We find a similar trend in our data. With an increase in preadsorbed water loadings, more CO_2 appears to react with water on the surface, which results in a CO_2 isotherm at low concentrations that shifts upward with a relatively higher partial pressure. Bertsch and Habgood also mentioned that carbon dioxide shows little chemisorption beyond approximately (0.5 to 1) molecule per cavity. For our zeolite 13X sample, with a chemical formula ($Na_{86}[(AlO_2)_{86}(SiO_2)_{106}]$) for unit cells and eight supercages per unit cell,[21] (0.5 to 1) molecule per cavity corresponds to (0.3 to 0.6) mol·kg^{-1}. Our data do not show much chemisorption above 0.3 mol·kg^{-1} but do show evidence for lower CO_2 loadings. Rege and Yang[4] observed a distinct enhancement in the amount of CO_2 adsorbed with H_2O at low concentrations on zeolite 13X for CO_2 concentration below 0.473 mg·L^{-1}, and the enhancement disappeared as the CO_2 partial pressure increased. The enhancement of CO_2 adsorption was explained by a catalytic formation of bicarbonate species on the adsorbent surface by adjacent H_2O molecules, or an enhancement of adsorbate diffusion due to the occupation of high energy sites by water molecules. It is noteworthy that the reported CO_2 loadings are less than 0.328 mol·kg^{-1} when the enhancement occurs, which agrees well with the previously calculated range.

Conclusions

Coadsorption equilibria have been measured for CO_2 and H_2O on zeolites 13X and 5A at temperatures of (0, 25, and 50) °C using a volumetric apparatus. The water loadings were held constant at (1.0, 3.4, and 9.4) mol·kg^{-1} and the CO_2 partial pressures varied. Binary adsorption is shown to be competitive for the pressure range studied, and the humidity results in dramatically reduced CO_2 capacities.

The binary adsorption of CO_2 on zeolites with water preloaded shows that the adsorbed amounts of CO_2 are higher than predictions at low CO_2 concentrations, and the trend is more obvious with an increase in water loadings and temperatures. On the basis of prior studies, this is caused by chemisorption promoted by the presence of water and the formation of carbonates or bicarbonates.

Binary equilibria have been compared with predictions of the IAST model with the Toth isotherm used to describe multitemperature pure component isotherms. The IAST gives a fair description for the adsorbed amount of CO_2 with low water loadings and temperatures, but shows a large discrepancy when water loadings and temperatures increase. The VEMC model has been applied to take into account the nonidealities with corrective terms for the IAST and gives satisfactory descriptions for all of the data using three virial excess mixing coefficients.

Literature Cited

(1) Bonenfant, D.; Kharoune, M.; Niquette, P.; Mimeault, M.; Hausler, R. Advances in Principal Factors Influencing Carbon Dioxide Adsorption on Zeolites. *Sci. Technol. Adv. Mater.* **2008**, *9*, 1–7.

(2) Dell'osso, L., Jr.; Winnick, J. Mixed-gas Adsorption and Vacuum Desorption of Carbon Dioxide on Molecular Sieve: Bed Design for Use in A Humid Atmosphere. *Ind. Eng. Chem. Process Des. Dev.* **1969**, *8*, 469–476.

(3) Rege, S. U.; Yang, R. T.; Buzanowski, M. A. Sorbents for Air Prepurification in Air Separation. *Chem. Eng. Sci.* **2000**, *55*, 4827–4838.

(4) Rege, S. U.; Yang, R. T. A Novel FTIR Method for Studying Mixed Gas Adsorption at Low Concentrations: H_2O and CO_2 on NaX Zeolite and γ-Alumina. *Chem. Eng. Sci.* **2001**, *56*, 3781–3796.

(5) Brandani, F.; Ruthven, D. M. The effect of Water on the Adsorption of CO_2 and C_3 H_8 on Type X Zeolites. *Ind. Eng. Chem. Res.* **2004**, *43*, 8339–8344.
(6) Bertsch, L.; Habgood, H. W. An Infrared Spectroscopic Study of the Adsorption of Water and Carbon Dioxide by Linde Molecular Sieve X. *J. Phys. Chem.* **1963**, *67*, 1621–1628.
(7) Montanari, T.; Busca, G. On the Mechanism of Adsorption and Separation of CO_2 on LTA Zeolites: An IR Investigation. *Vib. Spectrosc.* **2008**, *46*, 45–51.
(8) Coluccia, S.; Marchese, L.; Martra, G. Characterization of Microporous and Mesoporous Materials by the Adsorption of Molecular Probes: FTIR and UV-Vis Studies. *Microporous Mesoporous Mater.* **1999**, *30*, 43–56.
(9) Baltrusaitis, J.; Schuttlefield, J. D.; Zeitler, E.; Jensen, J. H.; Grassian, V. H. Surface Reactions of Carbon Dioxide at the Adsorbed Water-Oxide Interface. *J. Phys. Chem. C* **2007**, *111*, 14870–14880.
(10) Baltrusaitis, J.; Grassian, V. H. Surface Reactions of Carbon Dioxide at the Adsorbed Water-Iron Oxide Interface. *J. Phys. Chem. B* **2005**, *109*, 12227–12230.
(11) Li, G.; Xiao, P.; Webley, P. Binary Adsorption Equilibrium of Carbon Dioxide and Water Vapor on Activated Alumna. *Langmuir* **2009**, *109*, 10666–10675.
(12) Wang, Y.; LeVan, M. D. Adsorption Equilibrium of Carbon Dioxide and Water Vapor on Zeolites 5A and 13X and Silica Gel: Pure Components. *J. Chem. Eng. Data* **2009**, *54*, 2839–2844.
(13) Do, D. D. *Adsorption Analysis: Equilibria and Kinetics*; Imperial College Press: London, 1998.
(14) Myers, A. L.; Prausnitz, J. M. Thermodynamics of Mixed-Gas Adsorption. *AIChE J.* **1965**, *11*, 121–127.
(15) Yang, R. T. *Gas Separation by Adsorption Process*; Imperial College Press: London.
(16) Valenzuela, D. P.; Myers, A. L. *Adsorption Equilibrium Data Handbook*; Prentice Hall: Upper Saddle River, NJ, 1989.
(17) Qi, N.; LeVan, M. D. Virial Excess Mixing Coefficient Corrections for the Adsorbed Solution Theory. *Ind. Eng. Chem. Res.* **2005**, *44*, 3726–3732.
(18) Qi, N.; LeVan, M. D. Coadsorption of Organic Compounds and Water Vapor on BPL Activated Carbon. 5. Methyl Ethyl Ketone, Methyl Isobutyl Ketone, Toluene, and Modeling. *Ind. Eng. Chem. Res.* **2005**, *44*, 3733–3741.
(19) Lemmon, E. W. Vapor Pressure and Other Saturation Properties of Water. In *CRC Handbook of Chemistry and Physics*, 90th ed. (Internet version); Lide, D. R., Ed.; CRC Press/Taylor and Francis: Boca Raton, FL, 2010.
(20) Siriwardane, R. V.; Shen, M. S.; Fisher, E. P. Adsorption of CO_2, N_2, and O_2 on Natural Zeolites. *Energy Fuels* **2003**, *17*, 571–576.
(21) Walton, K. S.; Abney, M. B.; LeVan, M. D. CO_2 Adsorption in Y and X Zeolites Modified by Alkali Metal Cation Exchange. *Microporous Mesoporous Mater.* **2006**, *91*, 78–84.

Received for review January 18, 2010. Accepted May 16, 2010. This work was supported by the NASA Marshall Space Flight Center under Cooperative Agreement NNM07AA08A.

JE100053G